ACS Biomaterials SCIENCE & ENGINEERING

pubs.acs.org/journal/abseba

Letter

Self-Assembly of Solubilized Human Hair Keratins

Hui Ying Lai, Magdiel Inggrid Setyawati, Abdul Rahim Ferhan, Shiva Kamini Divakarla, Huei Min Chua, Nam-Joon Cho, Wojciech Chrzanowski, and Kee Woei Ng*

Cite This: https://dx.doi.org/10.1021/acsbiomaterials.0c01507

Read Online

ACCESS | Metrics & More | Article Recommendations | Supporting Information

ABSTRACT: Human hair keratins have proven to be a viable biomaterial for diverse regenerative applications. However, the most significant characteristic of this material, the ability to self-assemble into nanoscale intermediate filaments, has not been exploited. Herein, we successfully demonstrated the induction of hair-extracted keratin self-assembly in vitro to form dense, homogeneous, and continuous nanofibrous networks. These networks remain hydrolytically stable in vitro for up to 5 days in complete cell culture media and are compatible with primary human dermal fibroblasts and keratinocytes. These results enhance the versatility of human hair keratins for applications where structured assembly is of benefit.

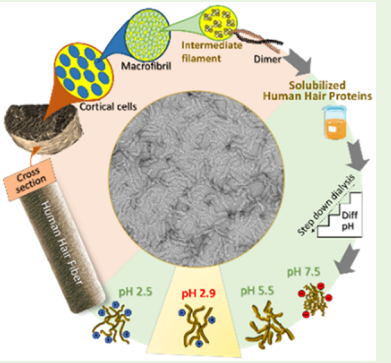

KEYWORDS: *self-assembly, keratin, coating, biomaterial, nanofibers*

Annual production of human hair biowaste has reached 750 million kg, making this a readily available source of keratins, which make up 80% of the total hair mass.[1] Because of the abundance, versatility, and reduced risk of interspecies pathogen transfer, cysteine-rich human hair keratins have emerged as a viable biomaterial with various potential applications in biomedical sciences.[2−6] Understanding the intrinsic behavior, interactions, and self-assembly characteristics of soluble human hair keratins will be pivotal to harnessing the full potential of this material. Much of the current understanding of cross-linking and hierarchical self-assembly of keratin intermediate filaments (IFs) was gleaned from epithelial keratins, from which peptide domains involved in the assembly were identified.[7,8] However, little of the same is known about human hair keratins, including the expression profiles of the various subtypes and the interaction mechanisms between them,[9−12] with only limited work done on selected recombinant hair keratins.[13] Herein, we report a method to induce the conformation change of hair keratin fibers by controlling the self-assembly process. This was achieved through a unique combination of pH and ionic control coupled with a step-down dialysis process. Keratins obtained via reductive extraction,[14] without going through additional purification steps, was observed to self-assemble into nanofibrous networks. This is the first successful in vitro attempt to simulate the native assembly process of hair extracted keratin IFs from solubilized monomers.

A two-step reductive extraction method[14] was adopted to first remove the keratin associated proteins (KAP) and subsequently dissociate and harvest total keratins from the "KAP-free hair". Purity of the keratin extracts was verified by the SDS-PAGE result which showed dominant presence of monomeric keratins in the samples, via the clear bands at about 45 kDa and 55 kDa (Figure S1). Previous reports utilizing a standard self-assembly buffer (phosphate buffer pH 7.5) had documented the reassembly and elongation process of recombinant hair and epidermal keratin fibers being governed by their different keratin subtypes.[7,8,13,15] A recent study also revealed the potential for extracted hair keratins to self-assemble into fibers, although these nanostructures were much thicker than regular keratin intermediate filaments and only a few micrometers long.[16] In contrast, we observed that chemically extracted total human hair keratins produced irregular mesh structures interspersed with globular aggregates (d < 6 nm) when phosphate buffer at pH 7.5 was introduced (Figure 1A, Figure 1B: I−III). Moreover, increased aggregation within the keratin network was observed with increasing buffer ionic strength (Figure S2). To produce uniform self-assembled keratin nanofibers, we employed a step-down dialysis process in acidic conditions (described in the Supporting Information). Thereafter, a self-assembly (SA) KCl solution (2.5 or 20 mM) was added to the dialyzed keratin solution for 1 h to further enhance the self-assembly capacity.

Received: October 20, 2020
Accepted: December 18, 2020

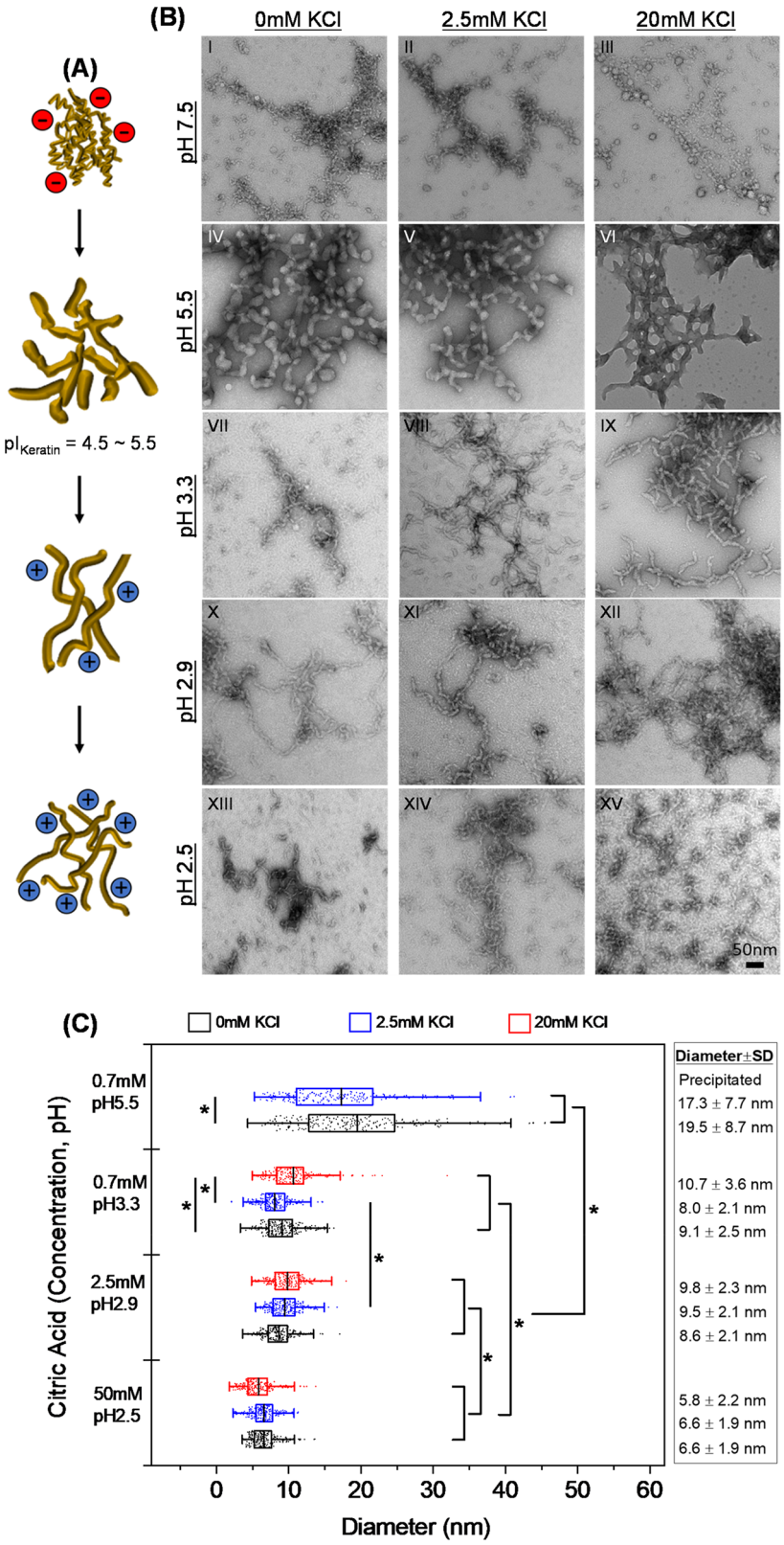

Figure 1. (A) Schematic of morphological and conformation changes of human hair keratins fibers in scale to the different pH conditions. (B) Representative TEM images of SA-keratins at different pH values and concentrations of KCl. Buffers up to pH 5.5 were prepared with Citric acid, whereas pH 7.5 buffer was prepared with 0.7 mM phosphate buffer (scale bar: 50 nm). (C) Box plots of SA-keratin nanofiber diameters across various self-assembly conditions. The minimum and maximum boundary lines of each box indicate the 25th and 75th percentile values, respectively. The lines within the boxes mark the mean values. Whiskers (above and below each box) indicate 1.5 IQR. Inset: Quantitative data of mean diameters ± SD (n = 200). *p < 0.05, two-way ANOVA, Tukey's HSD post hoc test.

https://dx.doi.org/10.1021/acsbiomaterials.0c01507
ACS Biomater. Sci. Eng. XXXX, XXX, XXX−XXX

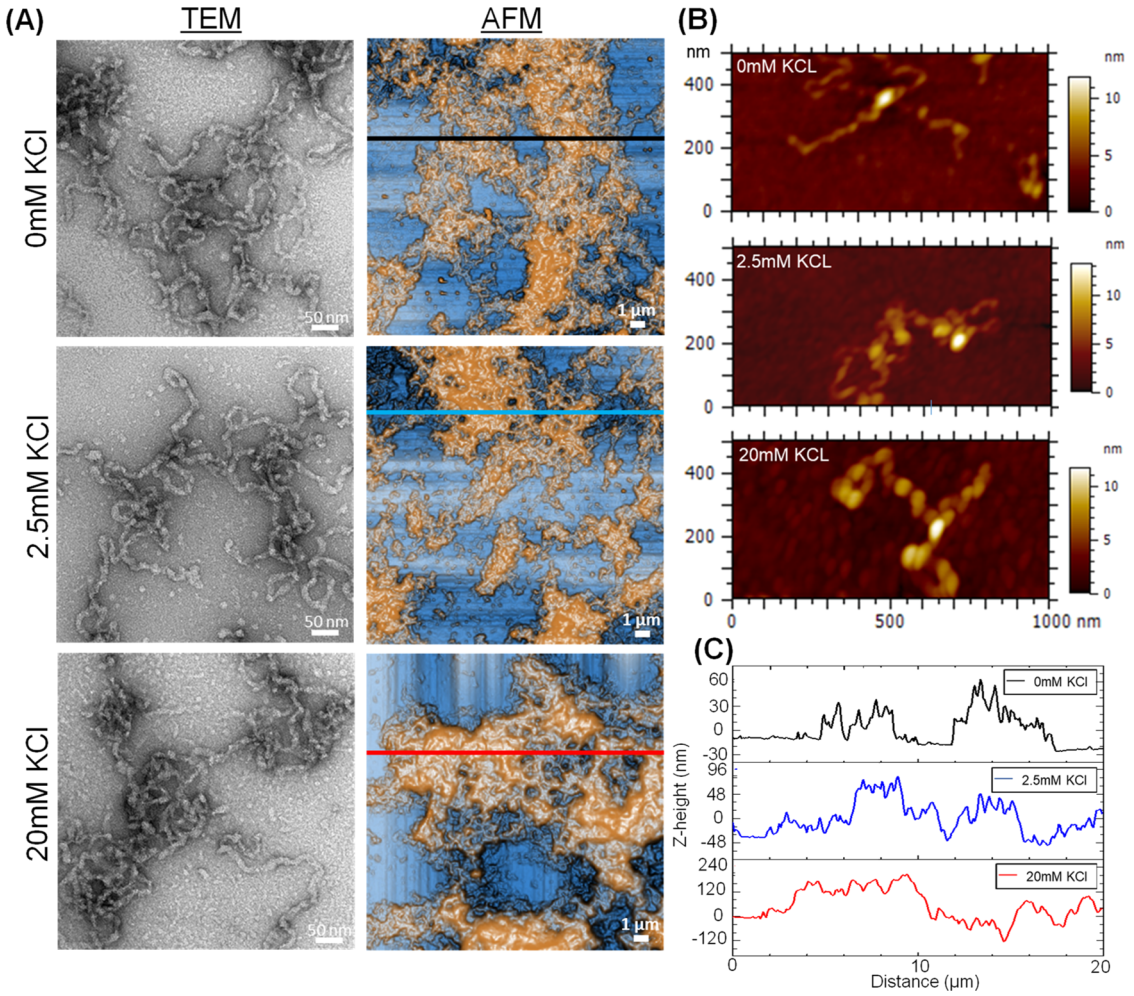

Figure 2. (A) Representative TEM and AFM images of SA-keratins prepared in 2.5 mM citric acid buffer (pH 2.9) following a 1 h self-assembly process. AFM images are presented in enhanced color mode. (B) Representative AFM images of individual SA-keratin fibers (pH 2.9) at higher magnification. (C) Z-height profile obtained from AFM line scans.

Finally, nanofiber structures with average diameters of 6−10 nm could be observed in acidic conditions prepared in 0.7−50 mM citric acid supplemented with 1 mM DTT (Figure 1B: VII−XV). Such slow and progressive conformation changes only occurred in gradual reduction of denaturant strength, as sparse and irregular aggregates were observed when the keratin extracts were directly dialyzed against water (Figure S3). It is worth noting that the step-down dialysis in acidic conditions could directly induce the self-assembly process without the addition of SA solution (Figure 1B: VII, X, XIII), indicating that the protonation of keratins is crucial to achieving thermodynamically favorable conditions for the self-assembly process. In acidic conditions (without SA), the nanofiber diameters were reduced proportionally with the buffer pH, as evidenced from the change in the average fiber diameter from 9.1 ± 2.5 nm to 6.6 ± 1.9 nm ($p < 0.01$) when the pH was reduced from 3.3 to 2.5 (Figure 1C). In contrast, increasing the salt concentration in the SA solution yielded significantly thicker fibers in 0.7 mM citric acid condition (pH 3.3). This was evidenced from the change of fiber diameter from 9.1 ± 2.5 nm to 10.7 ± 3.6 nm ($p < 0.01$) when salt concentration was increased from 0 mM to 20 mM (Figure 1B: VII, IX, Figure 1C). Increasing ionic strength through the introduction of salts was reported to induce lateral association of keratin filaments in vitro,[17,18] which competes with the filament elongation process.[18] Recently, the salt-induced charge screening effect was also reported to enhance the self-organization of wool keratin protofibrils.[16] Employing our proposed protocol, the assembled and elongated hair keratin nanofibers were found to be comparable to self-assembled purified epidermal keratins and specific recombinant hair keratin subtypes.[19,20] In basic conditions, the "locking" of basic head domains in keratins was previously described to inhibit proper filament assembly.[19] In contrast, the self-assembly propensity of our hair keratins was enhanced under protonated conditions in an acidic environment.

In natural hair fibers, keratin IFs present in the cortex region could range between 350 to 400 nm.[21−23] In the current study, the maximum length of traceable keratin fibers formed in acidic condition was around 380 nm, which is consistent with that of natural keratin IFs, although the majority of the keratin fibers formed were 50 to 130 nm long (Figure S4). It is worth noting that the accuracy of the length measurements could be compromised because of the highly entangled and intertwined nature of the assembled filaments. On the contrary, short fibers (<50 nm) with beaded ends and average diameter of 19.5 nm were observed when keratins were dialyzed at pH 5.5, possibly due to isoelectric point (keratin pI: 4.5−5.5) precipitation (Figure 1B: IV). Improved connectivity between the beads and bead elongation were observed under TEM upon the

https://dx.doi.org/10.1021/acsbiomaterials.0c01507
ACS Biomater. Sci. Eng. XXXX, XXX, XXX−XXX

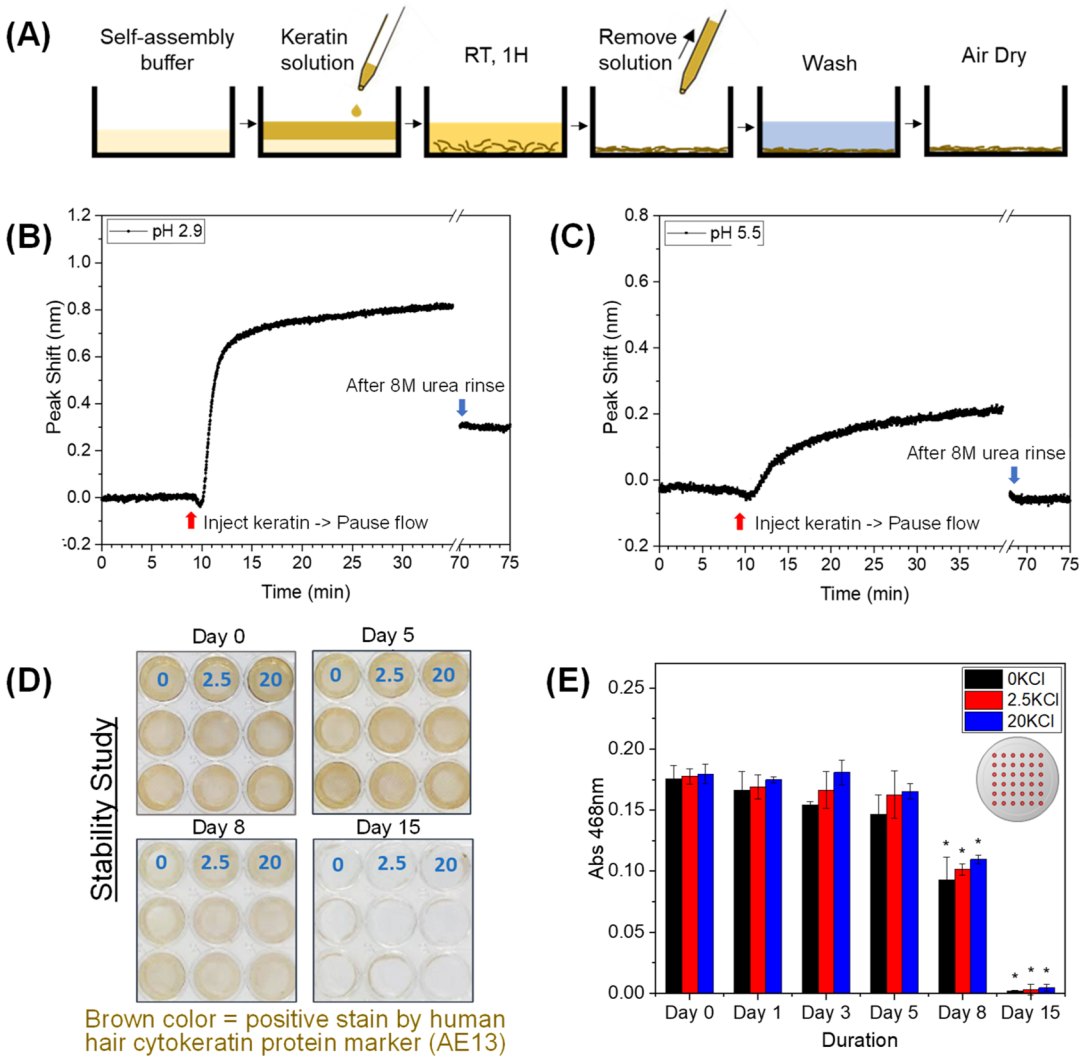

Figure 3. (A) Schematic showing the procedure of SA-keratin coating onto tissue culture plates. Indirect nanoplasmonic sensing (INPS) analysis to evaluate the efficacy of coating deposition using SA-keratin solution at (B) pH 2.9 and (C) pH 5.5 in the absence of KCl. (D) Immunoperoxidase staining of SA-keratin (pH 2.9) coating in complete DMEM media over 15 days and (E) their corresponding quantitative intensities. Data presented are means ± SD (n = 3). *p < 0.05, compare to day 0 of the corresponding sample group (one-way ANOVA, Tukey's HSD post hoc test).

introduction of 2.5 mM KCl, resulting in fiber networks of smaller fiber diameters (Figure 1B: V). High ionic charge, however, have been demonstrated to perturb the charges of the protein molecules and trigger aggregation.[24,25] This effect was specifically apparent when the environment pH approached the protein pI values, during which the protein becomes more susceptible to precipitation due to the reduction of stabilizing electrostatic repulsion forces. Indeed, agglomeration was observed upon addition of keratin solutions (at pH 5.5) into high salt content SA solutions, albeit network structures were maintained (Figure 1B: VI).

To verify that such self-assembly event was mainly pH dependent, we used 1.25 mM hydrochloric acid (HCl) and 55.3 mM acetic acid, in replacement of citric acid, to adjust the dialysis buffer to pH 2.9. Among the three acids tested, HCl showed the least buffering ability against high molarity urea, resulting in the precipitation of keratins during dialysis and the absence of any self-assembled fibers. Nonetheless, SA-keratin formed in 55.3 mM acetic acid, pH 2.9, condition showed comparable fiber diameters, which range from 8.1 to 8.9 nm, to the SA-keratin formed in 2.5 mM citric acid (Figure S5). Besides, across the acidic conditions tested, keratin solutions were found to precipitate during dialysis at pH 4.5, which fell within the range of the isoelectric points for hair keratins (Table S1). This underlines the crucial role of monitoring pH changes during the gradual urea removal dialysis steps in this self-assembly protocol. The correlation of average fiber diameters with pH, derived from representative transmission electron microscopy (TEM) images, can be found in Figures S5 and S6.

Among the acidic conditions tested in this study, the SA-keratin prepared in 2.5 mM citric acid (pH 2.9) showed the greatest homogeneity and consistency in term of fiber morphology and diameter. Hence, this condition was selected for the subsequent coating deposition and in vitro studies. Consistent with TEM observations, the SA-keratin nanofibers formed at this condition were observed as filamentous networks as well using atomic force microscopy (AFM) in enhanced color mode (Figure 2A). The Z-heights of the SA-keratin coatings were obtained using the AFM mapping

https://dx.doi.org/10.1021/acsbiomaterials.0c01507
ACS Biomater. Sci. Eng. XXXX, XXX, XXX−XXX

analysis (from original AFM images depicted in Figure S7). To ensure good observation and quantification of fiber morphology and diameter, we intentionally captured the images presented in Figures 1B and 2A at areas that were more sparsely coated with fibers. This led to a heterogeneous distribution of the coatings on silicon wafer, with the measured thickness of the entire layer ranging between 30 and 200 nm (Figure 2B). Nevertheless, at higher magnification under the AFM, individual fibers with larger diameters of 15−25 nm, compared with TEM analysis (8−10 nm), could be identified (Figure 2B). The larger fiber diameters observed in the coating format were a result of the tip broadening effect of AFM imaging.[26] Moreover, the SA-keratins were left for a relatively longer duration (1 h) during the fiber deposition stage, which allowed more extensive self-assembly. This led to a larger cluster of the self-assembled nanofibers compared to examination under TEM, where samples were loaded onto TEM grids for only 30 s. The thickness of the coating was further measured using a surface profilometer, which yielded comparable values to the AFM result (Figure S8). Further analysis with circular dichroism (CD) revealed that the SA-keratins were mainly composed of α helix domains (Figure S9).

Subsequently, the adsorption kinetics of SA-keratin coatings (Figure 3A) was monitored via indirect nanoplasmonic sensing (INPS).[27] SA-keratin fibers at pH 2.9 was observed to achieve pseudosaturation[28,29] 22 min after the flow was paused (Figure 3B). The deposition of SA-keratin coating was noted by the shift of the peak signal, which is proportional to the change in refractive index contributed by the adsorbed proteins. A higher initial absorption rate was observed in SA-keratin formed at pH 2.9 in contrast to the keratin at pH 5.5, evident from the steeper gradient (m = 0.499 vs. m = 0.036, Figure S10) captured from the 10th min onward. This could be attributed to the stronger electrostatic interaction between the positively charged SA-keratin (pH 2.9) and the sensor chip surface, compared to the neutral keratin at pI condition (pH 5.5). Moreover, an increment of 0.8 nm peak shifted was observed at the saturated point and further declined to 0.3 nm following the rinsing steps, which removed loosely bound keratin molecules. Close to 40% of the coating remained on the sensor chip even after extensive flushing, suggesting strong adhesion of keratins on the sensor chip. In contrast, under the same INPS experimental conditions, keratin at pH 5.5 showed a smaller peak shift at the saturation point (0.3 nm) and minimal attachment (11%) on the sensor chip after urea rinse (Figure 3C). This could be attributed to the charge effect and beadlike morphology that led to weaker adhesion of keratin molecules on the sensor chip surface (complete INPS profiles can be found in Figure S11). These observations further support the conclusion that 2.5 mM citric acid at pH 2.9 produced the most optimal self-assembled keratin fiber networks.

Coating stability and biocompatibility are the basic evaluation parameters required to understand their potential for biomedical applications. As such, we analyzed the stability of SA-keratin coatings in vitro in complete DMEM cell culture media at physiological temperature (37 °C). The successful formation of this uniform and good coverage SA-keratin coating (detailed in Figure 3A) could be observed by immunoperoxidase staining of broad spectrum human hair keratins. The positive stainings were relatively constant (Figure 3D, Figure S12) up to 5 days of incubation, suggesting stability of the coating over this time frame. Significant reduction in staining intensity was noted at day 8 (Figure 3D, Figure S12), when close to 50% reduction of the immunoperoxidase staining was registered (Figure 3E). Representative digital images revealed that coatings deposited at the center of the culture wells were effectively lost at day 15, confirmed by the significant reduction in immunoperoxidase staining based on absorbance mapping (Figure 3D, E).

In vitro biocompatibility of the SA-keratin coatings was tested with human dermal fibroblasts (HDF) and human epidermal keratinocytes (HEK), over the course of 5 days. The levels of metabolic activity of the cells grown on the coatings were comparable to controls cultured on untreated surfaces, as shown in Figures S13A, C. Keratin-derived biomaterials have been reported to facilitate wound healing and in more recent studies have been demonstrated to possess antioxidant properties.[5,30−34] In this study, a self-assembled 2D nanofibrous platform was fabricated using a low keratin concentration (0.5 mg/mL), demonstrating good adhesion and stability in physiological conditions. These preliminary results indicate that hair keratin coatings of self-assembled nanofibrous networks are easily produced and exhibit cell supporting capabilities. Moving forward, specific mechanistic analysis of the self-assembly process, cellular response to the SA-keratin coating and fabrication of bulk structures via the self-assembly process reported herein in comparison to other processing method[6,35−37] will be explored.

In summary, the first demonstration of the self-assembly potential of top down extracted human hair keratins into regular nanofibrous networks is presented. This was achieved in acidic conditions of pH $\leq$ 3.3, even without ionic induction through salt addition. A gradual decrease in fiber diameters from approximately 10 to 6 nm can be observed when the pH further reduced to pH 2.5. The SA-keratin at its optimal condition (2.5 mM citric acid, pH 2.9) was realized as biocompatible coatings by depositing the keratin solution in a static manner for 1 h. This coating remains stable in physiological conditions for up to 5 days. Altogether, the findings presented herein provide a new perspective into the self-assembly of human hair keratins in vitro, and serve as further impetus for future fundamental studies and development of human hair keratin-based biomaterial platforms.

EXPERIMENTAL SECTION

Step Down Dialysis. The acidic buffer solution used for keratin self-assembly was prepared using citric acid (Sigma). A range of citric acid concentrations (0.7, 2.5, and 50 mM in deionized water) were prepared at pH 2.9, 3.3, 4.5, and 5.5. NaOH was used to adjust the pH of 0.7 mM citric acid to achieve values of 4.5 and 5.5 (Table S1). 0.7 mM sodium phosphate buffer (pH 7.5) was used as the standard self-assembly protocol. For comparison, 0.125 mM hydrochloric acid and 55.3 mM acetic acid (Sigma) adjusted to pH 2.9 were used. The extracted keratin solution was first dialyzed against the corresponding buffer solution consisting of 8 M urea and 1 mM DTT overnight. Thereafter, the keratin solution was further dialyzed against the corresponding dialysis buffer by lowering the urea concentration in a stepwise manner, from 4 to 2 M urea for 3−4 h at each step. The keratin solution was left overnight in the final dialysis buffer (0 M Urea) for complete urea removal. All the above dialysis buffers contain 1 mM DTT.

Incorporation of Self-Assembly Buffer. The concentration of keratins after step down dialysis was determined using the Bradford assay (Biorad). The final concentration of keratins after being added to the self-assembly buffer was kept at 0.5 mg/mL. Initiation of self-assembly was performed by adding an equal volume of keratins to

https://dx.doi.org/10.1021/acsbiomaterials.0c01507
ACS Biomater. Sci. Eng. XXXX, XXX, XXX−XXX

either 5 or 40 mM KCl dissolved in the corresponding buffer solution (hereon referred to as SA solution), for a few minutes up to a few hours. Afterward, the self-assembled keratin was added to an equal volume of fixing solution containing 0.2% glutaraldehyde and 2.5 or 20 mM KCl for 3−5 min, and thereon ready to be applied to the intended surface to deposit the self-assembled networks. For cell culture and stability test purpose, the fixation step was eliminated. For TEM characterization, this was done on glow discharged carbon-coated grids and negatively stained with 2% uranyl acetate solution for before imaging (detailed protocol in Supporting Information). The final concentrations of KCl in the SA solution were either 2.5 or 20 mM dissolved in the corresponding citric acid buffer.

■ ASSOCIATED CONTENT

Supporting Information

The Supporting Information is available free of charge at https://pubs.acs.org/doi/10.1021/acsbiomaterials.0c01507.

Experimental procedures, SDS PAGE of the human hair keratin and KAP extracts, TEM, quantification of fibers' dimensions, AFM, surface profilometer, CD, INPS, and biocompatibility study (PDF)

■ AUTHOR INFORMATION

Corresponding Author

Kee Woei Ng − *School of Materials Science and Engineering, Nanyang Technological University, Singapore 639798, Singapore; Nanyang Environment & Water Research Institute (Environmental Chemistry and Materials Centre), Interdisciplinary Graduate Program, Nanyang Technological University, Singapore; Skin Research Institute of Singapore, Biomedical Science Institutes, Singapore 138648, Singapore; Department of Environmental Health, Harvard T.H. Chan School of Public Health, Boston, Massachusetts 02115, United States;* orcid.org/0000-0002-7276-3563; Email: kwng@ntu.edu.sg

Authors

Hui Ying Lai − *School of Materials Science and Engineering, Nanyang Technological University, Singapore 639798, Singapore; Nanyang Environment & Water Research Institute (Environmental Chemistry and Materials Centre), Interdisciplinary Graduate Program, Nanyang Technological University, Singapore;* orcid.org/0000-0002-9237-3001

Magdiel Inggrid Setyawati − *School of Materials Science and Engineering, Nanyang Technological University, Singapore 639798, Singapore*

Abdul Rahim Ferhan − *School of Materials Science and Engineering, Nanyang Technological University, Singapore 639798, Singapore;* orcid.org/0000-0003-3238-3125

Shiva Kamini Divakarla − *The University of Sydney, Sydney Nano Institute, Faculty of Medicine and Health, Sydney Pharmacy School, Sydney, New South Wales 2006, Australia*

Huei Min Chua − *School of Materials Science and Engineering, Nanyang Technological University, Singapore 639798, Singapore*

Nam-Joon Cho − *School of Materials Science and Engineering, Nanyang Technological University, Singapore 639798, Singapore;* orcid.org/0000-0002-8692-8955

Wojciech Chrzanowski − *The University of Sydney, Sydney Nano Institute, Faculty of Medicine and Health, Sydney Pharmacy School, Sydney, New South Wales 2006, Australia;* orcid.org/0000-0001-8050-8821

Complete contact information is available at: https://pubs.acs.org/10.1021/acsbiomaterials.0c01507

Author Contributions

H.Y.L. planned and executed the self-assembly experiments, did the TEM analysis, collated all data and wrote the manuscript. M.I.S. helped with data presentation and analysis. A.R.F. and N-J.C. planned, executed, and analyzed the INPS data. S.K.D. and W.C. planned and executed the AFM analysis. H.M.C. helped with sample preparation and biocompatibility studies. K.W.N. formulated the idea, provided the guidance and supervision, and helped analyze the data. All authors contributed to the writing and editing of the manuscript.

Notes

The authors declare no competing financial interest.

■ ACKNOWLEDGMENTS

This research is supported by the Agency for Science, Technology and Research (A*STAR) under its Acne and Sebaceous Gland Program & Wound Care Innovation for the Tropics IAF-PP (H17/01/a0/008 & H17/01/a0/0L9).

■ REFERENCES

(1) Gupta, A. Human Hair "Waste" and Its Utilization: Gaps and Possibilities. *J. Waste Manage.* **2014**, *2014*, 498018.

(2) Vasconcelos, A.; Cavaco-Paulo, A. The use of keratin in biomedical applications. *Curr. Drug Targets* **2013**, *14* (5), 612−619.

(3) Hartrianti, P.; Nguyen, L. T.; Johanes, J.; Chou, S. M.; Zhu, P.; Tan, N. S.; Tang, M. B. Y.; Ng, K. W. Fabrication and characterization of a novel crosslinked human keratin-alginate sponge. *J. Tissue Eng. Regener. Med.* **2017**, *11* (9), 2590−2602.

(4) Taraballi, F.; Wang, S.; Li, J.; Lee, F. Y. Y.; Venkatraman, S. S.; Birch, W. R.; Teoh, S. H.; Boey, F. Y. C.; Ng, K. W. Understanding the nano-topography changes and cellular influences resulting from the surface adsorption of human hair keratins. *Adv. Healthcare Mater.* **2012**, *1* (4), 513−519.

(5) Sow, W. T.; Lui, Y. S.; Ng, K. W. Electrospun human keratin matrices as templates for tissue regeneration. *Nanomedicine* **2013**, *8* (4), 531−541.

(6) Wang, S.; Wang, Z.; Foo, S. E. M.; Tan, N. S.; Yuan, Y.; Lin, W.; Zhang, Z.; Ng, K. W. Culturing fibroblasts in 3D human hair keratin hydrogels. *ACS Appl. Mater. Interfaces* **2015**, *7* (9), 5187−5198.

(7) Eichner, R.; Sun, T.-T.; Aebi, U. The role of keratin subfamilies and keratin pairs in the formation of human epidermal intermediate filaments. *J. Cell Biol.* **1986**, *102* (5), 1767−1777.

(8) Coulombe, P. A.; Fuchs, E. Elucidating the early stages of keratin filament assembly. *J. Cell Biol.* **1990**, *111* (1), 153−169.

(9) Hofmann, I.; Herrmann, H.; Franke, W. W. Assembly and structure of calcium-induced thick vimentin filaments. *Eur. J. Cell Biol.* **1991**, *56* (2), 328−341.

(10) Kreplak, L.; Aebi, U.; Herrmann, H. Molecular mechanisms underlying the assembly of intermediate filaments. *Exp. Cell Res.* **2004**, *301* (1), 77−83.

(11) Chrétien, D.; Metoz, F.; Verde, F.; Karsenti, E.; Wade, R. Lattice defects in microtubules: protofilament numbers vary within individual microtubules. *J. Cell Biol.* **1992**, *117* (5), 1031−1040.

(12) Moll, R.; Divo, M.; Langbein, L. The human keratins: biology and pathology. *Histochem. Cell Biol.* **2008**, *129* (6), 705−733.

(13) Parker, R. N.; Roth, K. L.; Kim, C.; McCord, J. P.; Van Dyke, M. E.; Grove, T. Z. Homo-and heteropolymer self-assembly of recombinant trichocytic keratins. *Biopolymers* **2017**, *107*, e23037.

(14) Fujii, T.; Takayama, S.; Ito, Y. A novel purification procedure for keratin-associated proteins and keratin from human hair. *J. Biol. Macromol.* **2013**, *13* (3), 92.

(15) Deek, J.; Hecht, F.; Rossetti, L.; Wißmiller, K.; Bausch, A. R. Mechanics of soft epithelial keratin networks depend on modular filament assembly kinetics. *Acta Biomater.* **2016**, *43*, 218−229.

(16) Cera, L.; Gonzalez, G. M.; Liu, Q.; Choi, S.; Chantre, C. O.; Lee, J.; Gabardi, R.; Choi, M. C.; Shin, K.; Parker, K. K. A bioinspired and hierarchically structured shape-memory material. *Nat. Mater.* **2020**, 1−8.
(17) Coulombe, P. A.; Bousquet, O.; Ma, L.; Yamada, S.; Wirtz, D. The 'ins' and 'outs' of intermediate filament organization. *Trends Cell Biol.* **2000**, *10* (10), 420−428.
(18) Kayser, J.; Grabmayr, H.; Harasim, M.; Herrmann, H.; Bausch, A. R. Assembly kinetics determine the structure of keratin networks. *Soft Matter* **2012**, *8* (34), 8873−8879.
(19) Herrmann, H.; Wedig, T.; Porter, R. M.; Lane, E. B.; Aebi, U. Characterization of early assembly intermediates of recombinant human keratins. *J. Struct. Biol.* **2002**, *137* (1−2), 82−96.
(20) Herrmann, H.; Häner, M.; Brettel, M.; Ku, N.-O.; Aebi, U. Characterization of distinct early assembly units of different intermediate filament proteins. *J. Mol. Biol.* **1999**, *286* (5), 1403−1420.
(21) Ahmadi, B.; Speakman, P. Suberimidate crosslinking shows that a rod-shaped, low cystine, high helix protein prepared by limited proteolysis of reduced wool has four protein chains. *FEBS Lett.* **1978**, *94* (2), 365−367.
(22) Jones, L. N.; Pope, F. M. Isolation of intermediate filament assemblies from human hair follicles. *J. Cell Biol.* **1985**, *101* (4), 1569−1577.
(23) Popescu, C.; Höcker, H. Hair—the most sophisticated biological composite material. *Chem. Soc. Rev.* **2007**, *36* (8), 1282−1291.
(24) Ozbas, B.; Kretsinger, J.; Rajagopal, K.; Schneider, J. P.; Pochan, D. J. Salt-triggered peptide folding and consequent self-assembly into hydrogels with tunable modulus. *Macromolecules* **2004**, *37* (19), 7331−7337.
(25) Carrick, L. M.; Aggeli, A.; Boden, N.; Fisher, J.; Ingham, E.; Waigh, T. A. Effect of ionic strength on the self-assembly, morphology and gelation of pH responsive β-sheet tape-forming peptides. *Tetrahedron* **2007**, *63* (31), 7457−7467.
(26) Keller, D. Reconstruction of STM and AFM images distorted by finite-size tips. *Surf. Sci.* **1991**, *253* (1−3), 353−364.
(27) Jackman, J. A.; Ferhan, A. R.; Yoon, B. K.; Park, J. H.; Zhdanov, V. P.; Cho, N.-J. Indirect nanoplasmonic sensing platform for monitoring temperature-dependent protein adsorption. *Anal. Chem.* **2017**, *89* (23), 12976−12983.
(28) Simonin, J.-P. On the comparison of pseudo-first order and pseudo-second order rate laws in the modeling of adsorption kinetics. *Chem. Eng. J.* **2016**, *300*, 254−263.
(29) Liu, Y. New insights into pseudo-second-order kinetic equation for adsorption. *Colloids Surf., A* **2008**, *320* (1−3), 275−278.
(30) Lai, H. Y.; Wang, S.; Singh, V.; Nguyen, L. T.; Ng, K. W. Evaluating the antioxidant effects of human hair protein extracts. *J. Biomater. Sci., Polym. Ed.* **2018**, *29* (7−9), 1081−1093.
(31) Bhardwaj, N.; Sow, W. T.; Devi, D.; Ng, K. W.; Mandal, B. B.; Cho, N.-J. Silk fibroin−keratin based 3D scaffolds as a dermal substitute for skin tissue engineering. *Integrative Biology* **2015**, *7* (1), 53−63.
(32) Wan, M.-Y.; Dong, G.; Yang, B.-Q.; Feng, H. Identification and characterization of a novel antioxidant peptide from feather keratin hydrolysate. *Biotechnol. Lett.* **2016**, *38* (4), 643−649.
(33) Xu, S.; Sang, L.; Zhang, Y.; Wang, X.; Li, X. Biological evaluation of human hair keratin scaffolds for skin wound repair and regeneration. *Mater. Sci. Eng., C* **2013**, *33* (2), 648−655.
(34) Kelly, R.; Ellis, G.; Macdonald, R.; McPherson, R.; Middlewood, P.; Nuthall, M.; Rao, G.-F.; Roddick-Lanzilotta, A.; Sigurjonsson, G.; Singleton, D. Keratin and soluble derivatives thereof for a nutraceutical and to reduce oxidative stress and to reduce inflammation and to promote skin health. U.S. Patent Application 11/370 063, 2007.
(35) Chua, H. M.; Zhao, Z.; Ng, K. W. Cryogelation of Human Hair Keratins. *Macromol. Rapid Commun.* **2020**, *41* (21), 2000254.
(36) Zhao, Z.; Moay, Z. K.; Lai, H. Y.; Goh, B. H. R.; Chua, H. M.; Setyawati, M. I.; Ng, K. W. Characterization of Anisotropic Human Hair Keratin Scaffolds Fabricated via Directed Ice Templating. *Macromol. Biosci.* **2020**, 2000314.
(37) Wang, S.; Taraballi, F.; Tan, L. P.; Ng, K. W. Human keratin hydrogels support fibroblast attachment and proliferation in vitro. *Cell Tissue Res.* **2012**, *347* (3), 795−802.

https://dx.doi.org/10.1021/acsbiomaterials.0c01507
ACS Biomater. Sci. Eng. XXXX, XXX, XXX−XXX